

M. Clavel* and X. Feaugas*

Micromechanisms of Plasticity under Multiaxial Cyclic Loading

REFERENCE Clavel, M. and Feaugas, X., *Micromechanisms of plasticity under multiaxial cyclic loading*, **Multiaxial Fatigue and Design**, ESIS 21 (Edited by A. Pineau, G. Cailletaud, and T. C. Lindley) 1996, Mechanical Engineering Publications, London, pp. 21-41.

ABSTRACT An attempt is made to clarify the situation concerning deformation modes operative under non-proportional cyclic loadings. We will first discuss the influence of the stacking fault energy in relation to cross-slip on the mechanical behaviour of alloys. We will show that these parameters are not fully effective in precipitate-strengthened alloys. The influence of the friction stress and the back stress will be discussed later. We will point out that in dual phase alloys, the influence of complex loading paths is not yet understood. It is shown that a considerable amount of work remains to be done for a better knowledge of micromechanisms of plasticity under complex non-proportional loading paths in order to develop an appropriate model in the future.

1 Introduction

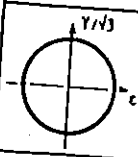

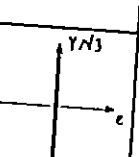
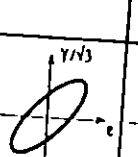
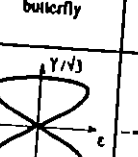
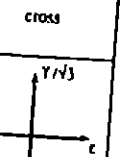
In the past, much work was carried out using various materials on the influence of complex loading paths on the micromechanisms of plasticity. It was shown that some alloys can exhibit overstrengthening or oversoftening effects under non-proportional loading paths. The amount of strengthening or softening depends on various physical parameters and it was pointed out that the stacking fault energy and above all the cross-slip propensity play a major role in FCC alloys.

In accordance with the rotation of the stress principal axis during out-of-phase tests, slip activity on multiple slip systems is required for strain accommodation (1). This slip multiplicity was clearly demonstrated by several authors in various alloys (2-4). This effect was quantified in nickel-base alloys (4, 7) and aluminium alloys (5, 6). It was shown that overstrengthening is linked to slip multiplicity, but some confusion appears on comparing all the results, particularly on the microscopic scale.

For the sake of simplicity we have to summarize firstly the most common loading paths in Table 1 using the von Mises strain space ($\epsilon(t), \gamma(t)/\sqrt{3}$). Whatever the loading path, the axial strain $\epsilon(t)$ and the shear strain $\gamma(t)$ are defined as follows:

*UTC, LG2ms, Division mécanique, URA CNRS 1505, Centre de Recherche de Royallieu, BP 649, 60206 Compiègne, France.

Table 1 Schemes of various loading paths in the space ($\gamma/\sqrt{3}, \epsilon$).

TTQ	ATC	ATT		butterfly	cross
					
Tension-torsion $\phi = \pi/2$	Tension-compression $\gamma = 0$	Alternating torsion $\epsilon = 0$	Tension-torsion $\phi = \pi/6$	Tension-torsion $\phi = 0$ $q = 2$	Tension-compression and torsion alternately

$$\epsilon(t) = \epsilon_0 \sin(q\omega t)$$

$$\gamma(t) = \gamma_0 \sin(\omega t - \phi)$$

$$\lambda = \gamma_0/\epsilon_0$$

except for the cross-test corresponding to tension-compression alternately with torsion-torsion (a zero equivalent von Mises strain was imposed at the beginning of each alternation); γ_0 and ϵ_0 are the amplitudes of strains, ω the frequency of oscillation and ϕ is the phase lag between the two sinusoidal signals. All the tests were conducted with $q = 1$, except the butterfly test which was conducted with $q = 2$.

It was clearly demonstrated that the greatest overstrengthening effects were obtained with a phase lag equal to 90° and a ratio $\lambda = \sqrt{3}$ (8). Nevertheless, other tests which qualify as non-proportional enhance overstrengthening, for example the cross-test or the butterfly test (9).

2 Cyclic Stress Evolution in Terms of Latent Hardening

It has been widely observed that the amount of cyclic hardening increases significantly for materials such as copper or stainless steels under non-proportional cyclic loadings, whereas other materials such as aluminium exhibit the same amount of hardening under both proportional and non-proportional cyclic loadings (3, 10). Dislocation substructures of metals resulting from non-proportional cyclic loadings have been investigated by different authors (3, 10-15). Various kinds of substructures were reported: veins, walls, persistent slip bands (PSB), labyrinths, cells, twins, etc. Generally these observations were made on polycrystalline materials and some authors compared their results with those obtained on monocrystalline samples. Furthermore, even in single crystals, the deformation modes will depend on the loading path, the plastic strain amplitude ($\Delta\epsilon_p/2$), the cumulative plastic strain (P_{cum}) and the stacking

fault energy (SFE). To some extent, in polycrystals the grain boundaries and the orientation of grains i.e. crystallographic textures may play a major role and between the interior of grains and in the grain boundaries vicinity, different deformation modes are expected to appear.

To compare the various results reported in the literature regarding the influence of non-proportional loading paths, we have basically to define the types of deformation mode which are generally encountered under proportional loading paths.

For the sake of simplicity we must define firstly the microstructural features and their mechanical behaviour under straining. For this purpose the main deformation modes which were observed are reported in Table 2 as functions of the plastic strain amplitude and the cumulative plastic strain. We use the terminology defined elsewhere (16–18). Typical microstructures observed in polycrystals are shown in Fig. 1.

Table 2 Denomination of the most common dislocations arrangements, for increasing values of $\Delta\epsilon_p/2$ or P_{cum} .

Phase	Planar slip bands or dipoles and multipoles or/and tangles	Matrix (simple slip)	Wall	Cell
Structure		Veins Channels	PSB-Ladder (simple slip) Labyrinth (multiple slips)	Cell

In the matrix phase, veins (high density of dislocations, $\rho = 3.10^{15}$) and channels (weak density of dislocations, $\rho = 10^{12}$) have the same volume fraction. The veins primarily consist of edge dislocations with an average Burgers vector very close to zero. Thus the veins do not produce a long-range internal stress under a zero applied stress (19). At finite applied loads large internal stresses are expected to appear due to the *polarization* of dipoles patches. As the applied stress increases, the vein structure becomes unstable and it was calculated that the Nabarro–Taylor lattice evolves to form walls ($\rho = 2.10^{15}$ to 6.10^{15}) and channels ($\rho = 10^{13}$) (wall phase) typical of the ladder-like structure of persistent slip bands (PSB). These two phases, namely the matrix (veins and channels) and the wall (walls and channels) are associated with single slip. When two slip systems are required to accommodate the deformation, it was observed that the labyrinth dipolar wall structure occurs, resulting from double polygonization arrangements of edge in character dipolar loops with two Burgers vectors on any of the two activated slip systems (20, 21). Moreover, as the deformation proceeds or as the applied strain increases, a cellular network takes place. These latter structures are associated with multiple slips and/or dislocation cross slip. It was shown that a PSB or a labyrinth structure could evolve progressively into cells during extensive cycling (18, 22). Then it appears that wall and labyrinth

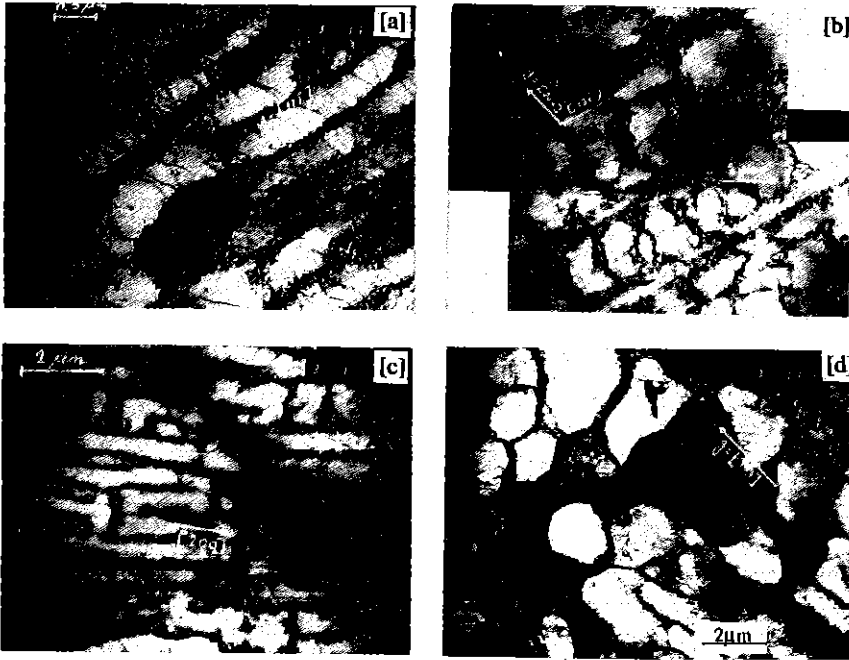


Fig 1 Transmission electron microphotograph showing the structures defined in Table 2: (a) veins; (b) PSB; (c) Labyrinths; (c) Cells-316-type austenitic stainless steel (22).

structures have to be considered as transient phenomena (22). Nevertheless these structures are obviously associated with a characteristic slip multiplicity. As it was formerly explained for veins, each microstructure would be associated with particular long range stresses (23).

The propensity of the material needed to exhibit the preceding microstructures strongly depends on the stacking fault energy (γ).

It was shown that in high SFE materials (aluminium for example) the deformation proceeds mainly from cell formation in a wide range of applied strains (24, 25), whereas for low SFE materials, planar slip takes place and cell formation occurs only at large applied strains (22, 26, 27). Then it clearly appears that the ratio $\gamma/(\mu b)$ is a better parameter than the stacking fault energy ($\mu =$ shear modulus, $b =$ Burgers vector) (28). The ratio $\gamma/(\mu b)$ is related to the stacking fault ribbon width, which generally characterizes the cross-slipping ability of FCC materials. As previously proposed, the deformability of the cyclic structures (veins, ladders, labyrinths, cells etc.) should be characterized by the ratio P of the volume occupied by the hard zones (ex. walls) divided by the volume occupied by the soft zones (ex. channels) (29). The value of the ratio P is about 0.5 for veins and 0.1 for labyrinths and PSB. This ratio decreases when the cell structures appear in the matrix.

In fact the structures which were defined above would be simultaneously observed in cyclically strained polycrystals. Nevertheless, in the following we will try to discuss the average microstructures which were reported by various authors. As shown previously (16, 18, 29), in polycrystals the cyclic microstructure may evolve following a trend similar to the one observed in monocrystals. Several results obtained by various authors are included in Tables 3 and 4 which refer respectively to proportional and non-proportional loading paths. In these tables are also indicated the stacking fault energy, the ratio $\gamma/(\mu b)$ and the applied plastic strain range corresponding to the tests.

Table 3 Deformation modes in FCC alloys under proportional loading paths: the stacking fault energy (SFE), the strain range ($\Delta\epsilon_{pequ}$ VM/2) and the authors, are also indicated.

Metals and solid solution alloys	SFE (mJm ²)	$\gamma/(\mu b)$ (10 ⁻³)	2 × 10 ⁻⁵	10 ⁻⁴	10 ⁻³	10 ⁻²	Ref.
			---+-----+-----+-----+-----+ 5 × 10 ⁻⁵	-----+-----+-----+-----+ 5 × 10 ⁻⁴	-----+-----+-----+-----+ 2 × 10 ⁻³	$\Delta\epsilon_p/2$	
Al(pure), Al-Mg, Al 6061	135	18.9	+-----+ Cells		+-----+ Cells		(24)(10) (3)
Al-0,7%Li			+-----+-----+-----+-----+ Uncondensed Elongated cells Cells Cells Cells Labyrinth Walls-Channels				(29)
Ni (pure)	125	6.3			+---+ Cells		(3)
Cu (pure)	45	3.8	---+-----+-----+-----+ Dipoles PSB PSB Veins Labyrinths			Cells	(15)
Co44Ni	45	2.55			+-----+ Walls-channels Elongated cells		(32)
310	40	1.76			+-----+ Planar slip Some walls		(10)
316L	25	1.1	Dipoles, Multipoles Planar slip	Tangles, Veins Some cells	PSB Cells twins	Cells-- Labyrinths	(22) (2, 15) (30)
304	20	0.88	+-----+ Planar slip Some walls		+---+ Elongated Cells Cells		(3)(10)
Co33Ni	15	0.85	+-----+-----+-----+ Patches		+-----+ Walls-Channels Cells		(32)

Table 4 Deformation modes in FCC alloys under non-proportional loading paths (TTQ and Cross): the stacking fault energy (SFE), the strain range ($\Delta\epsilon_{pequ}$ VM/2) and the author's, are also indicated.

Metals and solid solution alloys	SFE (mJm ⁻²)	$\gamma/(\mu b)$ (10^{-3})	2×10^{-5}	10^{-4}	10^{-3}	10^{-2}	$\Delta\epsilon_{pequ}/2$	Ref.
			-----+-----+-----+-----+	-----+-----+-----+-----+	-----+-----+-----+-----+	-----+-----+-----+-----+		
Al (pure) Al 6061	135	18.9	-----+-----+-----+-----+	-----+-----+-----+-----+	-----+-----+-----+-----+	-----+-----+-----+-----+		(10)(3)
			Cells TTQ AH = 0%		Cells Cross AH = 0%			
Ni (pure)	125	6.3			-----+-----+-----+-----+	-----+-----+-----+-----+		(3)
					Cells Cross AH = 27%			
Cu (pure)	45	3.8	-----+-----+-----+-----+	-----+-----+-----+-----+	-----+-----+-----+-----+	-----+-----+-----+-----+		(10)(3)
			Labyrinths Uncondensed cells I cells TTQ 30% < AH < 50%		Cells Cross AH = 22%			
Co44Ni	45	2.55		-----+-----+-----+-----+	-----+-----+-----+-----+			(32)
				Cells TTQ AH < 28%	Cells AH = 47%			
310	40	1.76		-----+-----+-----+-----+	-----+-----+-----+-----+			(10)
				Cells-Labyrinths TTQ 28% < AH < 55%				
316L	25	1.1		-----+-----+-----+-----+	-----+-----+-----+-----+	-----+-----+-----+-----+		(15)(30) (34)(31)
				Cells-twins TTQ 20% < AH < 72%				
304	20	0.88	-----+-----+-----+-----+	-----+-----+-----+-----+	-----+-----+-----+-----+	-----+-----+-----+-----+		(10)(3)
			Cells-Labyrinths TTQ 31% < AH < 58%		Cells Cross AH = 22%			
Co33Ni	15	0.85		-----+-----+-----+-----+	-----+-----+-----+-----+	-----+-----+-----+-----+		(32)
				Cells-Stacking faults TTQ 15% < AH < 28%				

The comparison of the deformation microstructures observed under proportional loading paths (Table 3) and under non-proportional loading paths (Table 4), shows clearly that the structures of dislocations which are linked to slip multiplicity (labyrinths and cells) appear at a smaller plastic strain during non-proportional loading than during proportional loading. Broadly speaking, it is observed that the overstrengthening effect is associated with a decrease in the P-ratio corresponding to the domain in which deformation modes are characterized by veins or PSB and labyrinths. On the contrary, in the domain in which cells take place, it was observed that the overstrengthening effect goes hand-in-hand with decrease in cell size.

A careful examination of Table 4 clearly shows that the dependence on the non-proportional overstrengthening effect is associated, on the one hand, to the $\gamma/(\mu b)$ ratio and, on the other hand, to the applied plastic strain. Figure 2 shows

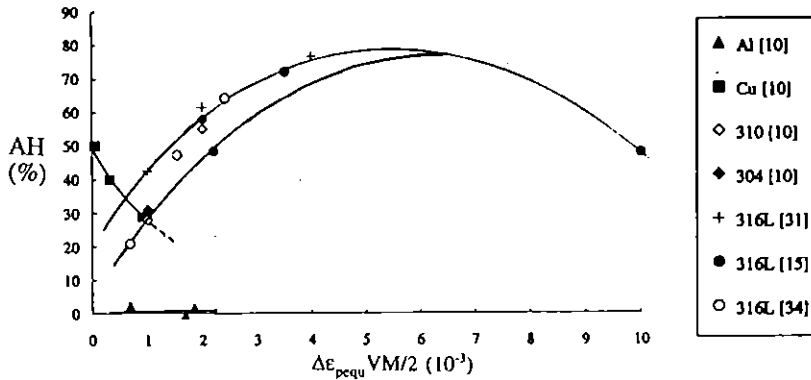


Fig 2 Variation of additional hardening ratio vs the von Mises equivalent plastic strain.

the main results obtained with the out-of-phase loading paths in a wide range of applied plastic strains for a large variation of the $\gamma/(\mu b)$ ratio. The overstrengthening phenomenon can be quantified with the additional hardening ratio measured at a given equivalent plastic strain.

$$AH = \frac{100(\Sigma_{\text{non proportional}} - \Sigma_{\text{proportional}})}{\Sigma_{\text{proportional}}}$$

Firstly let us consider the case of copper for which the AH ratio increases as the applied strain decreases (Fig. 2). In fact this effect is fairly well correlated with slip multiplicity. Generally, the slip multiplicity increases with the plastic strain amplitude range in proportional loading paths. The overstrengthening effect being linked to the slip multiplicity, there is a plastic strain level at which the overstrengthening effect associated with the non-proportional loading path decreases when the applied plastic strain increases. It appears that the maximum of the AH ratio would correspond to the transition between the PSB structure under proportional loading paths to the cell structure under non-proportional loading paths. A similar comment could be made about the mechanical behaviour of various austenitic stainless steels. Schematically one can consider that the higher the slip multiplicity from ATC-TTQ the higher the overstrengthening and that the decrease in SFE enhances this phenomenon. In the same way, it is interesting to plot the whole result in terms of latent hardening.

Following the results obtained elsewhere, Fig. 3(a) (33), we report in Fig. 3(b) the variation of the AH ratio as a function of the ratio $\gamma/(\mu b)$. At $\gamma/(\mu b) > 1.1$, it appears that easy cross slip (a narrow stacking fault ribbon) reduces the overstrengthening effect (AH). Nevertheless at very low $\gamma/(\mu b)$ ratio ($\gamma/(\mu b) < 1.1$ - left part of the curve) it would seem that AH could decrease when the $\gamma/(\mu b)$ ratio decreases as suggested by the results obtained on Co-33Ni (32). This fact is not at the present time very well established and therefore it necessitates further work.

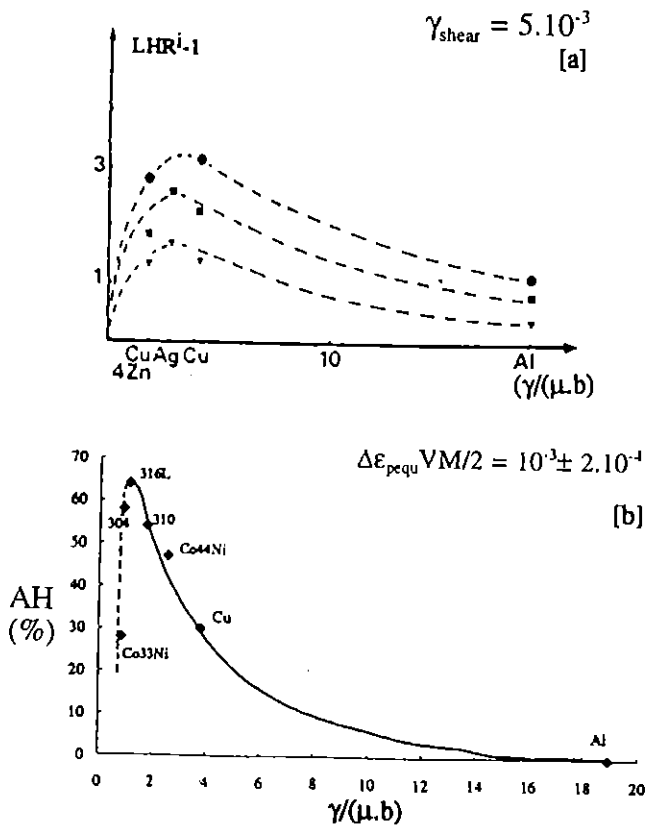


Fig 3 Influence of the ratio $\gamma/(\mu b)$: (a) on latent hardening under tension tests (33), and (b) on overstrengthening under non-proportional cyclic tests.

A similar behaviour was observed elsewhere (33) about the latent hardening anisotropy (Fig. 3(a), $LHR^i = \tau_c^{si}/\tau_c^p$, τ_c^{si} = initial CRSS on the i secondary active system, τ_c^p = final CRSS on the primary active system). Nevertheless the maximum of the hardening anisotropy observed in Fig. 3(a) was obtained for $\gamma/(\mu b)$ ratio corresponding to the value associated with silver, i.e. $\gamma/(\mu b) = 2.6$. In our case, the AH ratio maximum is observed at $\gamma/(\mu b) = 1.1$. In our opinion such a discrepancy could originate from the decomposition of the AH ratio in friction and back stresses. The maximum hardening anisotropy and/or the maximum overstrengthening effect suggest that a critical dislocation dissociation could exist. It can be interpreted as follows: in the domain of higher $\gamma/(\mu b)$ the partial dislocations move together and have to recombine for cross-slipping. In the low $\gamma/(\mu b)$ domain, the stacking fault ribbon is large enough to allow the independent motion of the partial dislocations and the obstacle can be just passed without any need of the recombination process (33). Nevertheless, we

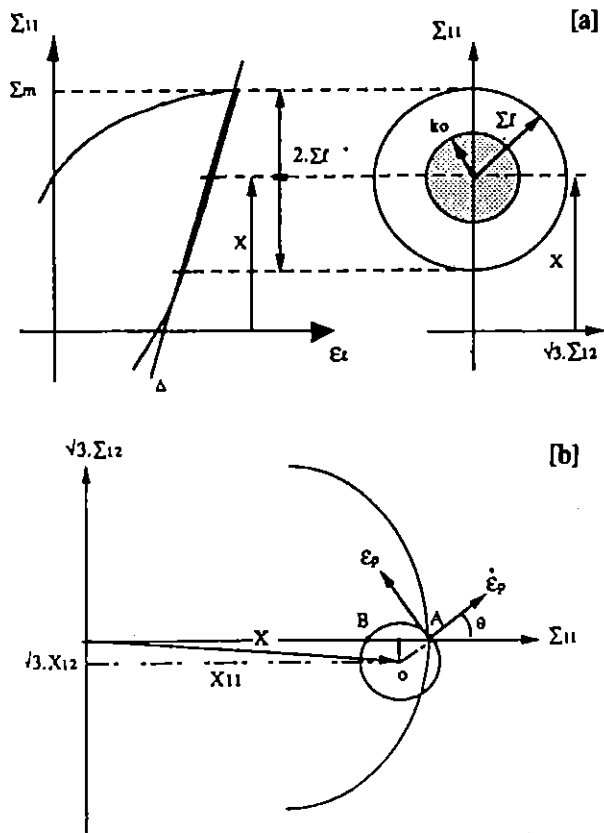


Fig 4 Diagrams showing the partitioning of cyclic stress: (a) back stress (X) and friction stress (Σ_f) shown on the hysteresis loop; (b) location of A and B points in the stress space.

must keep in mind, that a very low SFE, will favour mechanical twinning and/or martensitic transformations. These deformation modes are expected to favour the overstrengthening effect. From the studies in which mechanical twinning is reported, it appears that under out-of-phase loading paths, twinning deformation occurs at a relatively low plastic strain (15). This fact agrees with the existence of a critical stress corresponding to twinning nucleation (15).

In some studies the effect of temperature was also examined (34). Mechanical results and dislocation configurations are in agreement with the fact that a temperature increase will enhance the stacking fault energy, and overstrengthening will progressively vanish. From this first part it appears that the ratio $\gamma/(\mu b)$ and the slip multiplicity could partly explain the mechanical behaviour under complex loadings.

Cyclic Stress Evolution in Terms of Back Stress and Friction Stress

Nevertheless this approach is partially inadequate. It has recently been shown that cross-slip is not only dependent on the $\gamma/(\mu b)$ ratio, but also on short-range order or short-range clustering in solid solutions, precipitate shearing, and dynamic steady-state separation of partials (35–37). It has been shown previously that slip multiplicity enhances overstrengthening, but this latter could originate either from a friction stress or from a back stress and more generally from cyclic dislocation features, which are often very well defined. As a matter of fact, heterogeneous deformation structures enhance long-range stresses (23). Very few results have been reported to account, on the one hand, the short-range dislocation interactions and, on the other hand, the long-range stresses. So far the overstrengthening effect under complex loadings was modelled essentially at the isotropic level using an interaction matrix in the writing of the isotropic component (rs) on slip systems (38), i.e.

$$rs = q \text{ Som}_{r \in S} \{h_{rs} [1 - \exp(-bv_r)]\}$$

where rs represents the isotropic component of the hardening on s system h_{rs} is a component of the interaction matrix and v_r is the accumulated viscoplastic shear strain on each system r , while b is a numerical constant.

This procedure was very fruitful but not really representative of the mechanical behaviour. Partitioning of the cyclic stress in a back stress and a friction stress must be carried out for a better understanding of the micromechanisms of plasticity under complex loading paths.

Back Stress (X) and Friction Stress (Σ_f) Measurements

These concepts are very common in the literature, but there is no precise definition of these stresses, each author having his own point of view. In the present paper, as a definition of back stress, we will consider the stress associated with a local strain process which induces a long-range interaction with mobile dislocations. The friction stress is the stress required locally for a dislocation to move.

Numerous experimental methods to determine back stress and friction stress were reported in the literature (dip-test, relaxation-test, Cottrell method, etc.) specially for proportional loading paths (39–43). On the contrary, these stress component measurements are seldom undertaken under non-proportional loading paths. In fact such measurements need the removal of one component of straining.

The stress partition, previously proposed by Cottrell (41), and discussed in the past by Kuhlmann-Wilsdorf (42) is carried out on a hysteresis loop. The principle of this method is described in Fig. 4a. Nevertheless, this partition necessitates a strong hypothesis: the activated back stress in the elastic domain

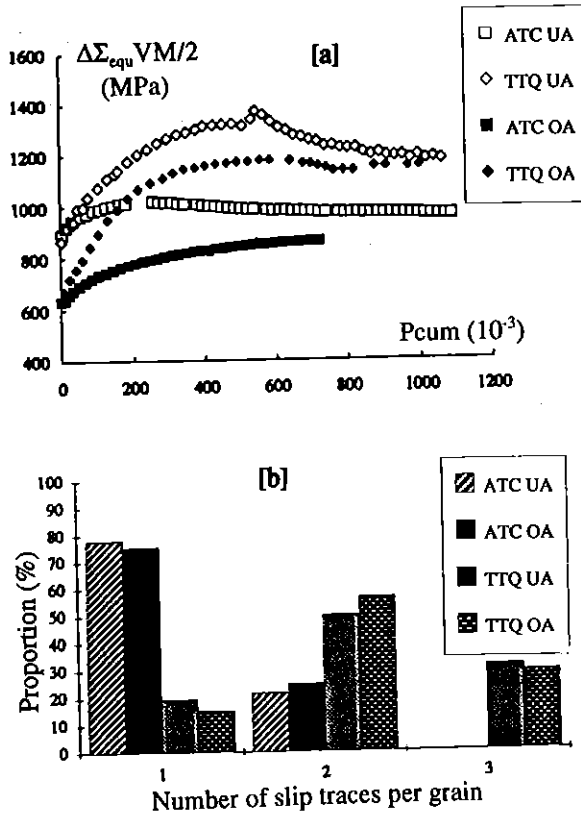


Fig 5 Cyclic behaviour of a Ni-base alloy ($\Delta\varepsilon_{peq} VM/2 = 0.45\%$) (7): (a) evolution of the equivalent stress vs the cumulated strain; (b) number of slip traces per grain.

(between A and B points) must remain constant during back straining. Some parameters, like temperature, plastic strain rate, or mechanical control (total strain or plastic strain) can break this hypothesis. Further comments on this subject are available in a specific publication (43). Furthermore Cottrell's method gives information on the value of the back stress, X , corresponding to a particular state of stress, although no information is available on X -rate. Nevertheless in the following we will consider that Cottrell's method allows reliable measurements of the back stress (X), to be obtained as only comparative results are discussed.

Some authors (6, 7) obtained values of the back stress and the friction stress temporarily removing the shear stresses component. Then Cottrell's method can be used on the tension-compression hysteresis loop. In fact, to obtain a stabilized hysteresis loop, many cycles in-phase are required which generally induce a softening period. This method allows a back stress and a friction stress associated with a residual overstrengthening to be identified. Another alternative

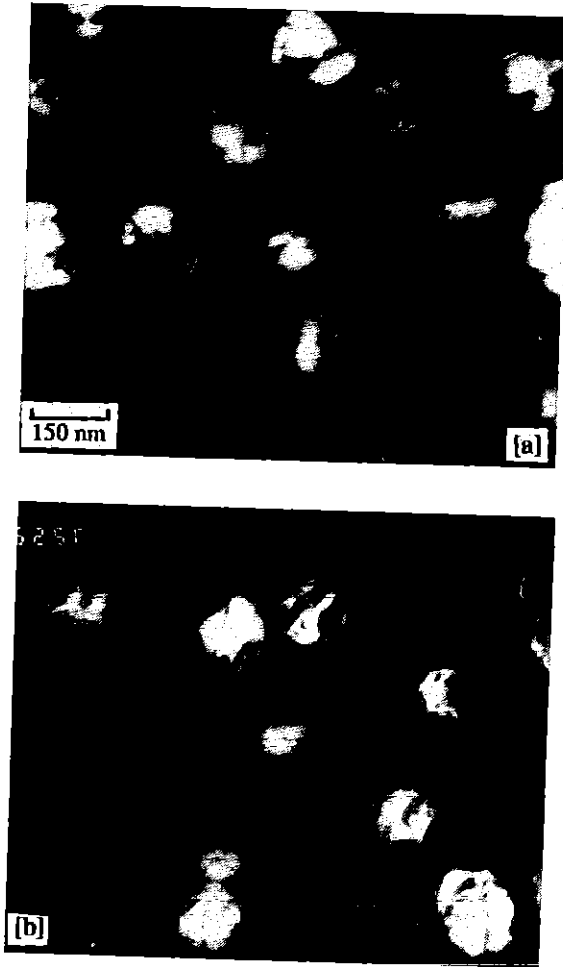
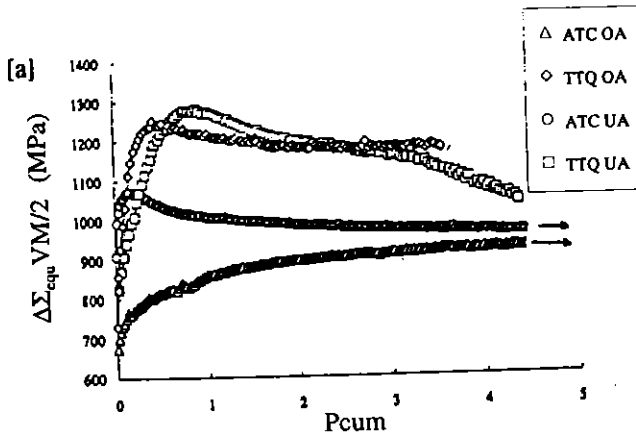


Fig 6 Deformation modes in a Ni-base alloy (7): (a) under a proportional loading path; (b) under a non-proportional loading path.

can be proposed which involves identification of the B-point location and the measurement of θ angle (Fig. 4b). B location is obtained by reversing the tension stress under a nil shear stress. θ is the angle between the plastic strain rate and the tension axis at A-point.

This approach was used in solid solution alloys (32, 44) and it was shown that the overstrengthening effect can originate either essentially from the back stress for Co33Ni or from both friction stress and back stress components for Co45Ni.

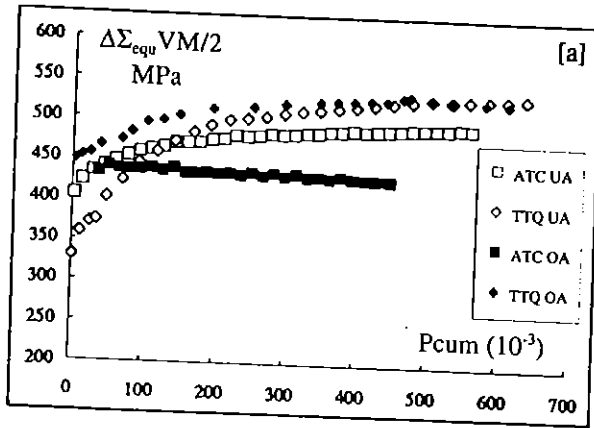
These measurements were made on two metallurgical conditions in Waspaloy which is a precipitate-strengthened alloy. The underaged state (UA) corresponds



[b]	ATC	TTQ
U.A. k = 850 MPa	ΣeqVM = 939 MPa R = - 205 MPa X = 294 MPa	ΣeqVM = 1315 MPa R = 98 MPa X = 367 MPa
O.A. k = 580 MPa	ΣeqVM = 859 MPa R = - 150 MPa X = 429 MPa	ΣeqVM = 1115 MPa R = - 10 MPa X = 545 MPa

Fig 7 Cyclic behaviour of Ni-base alloy ($\Delta\epsilon_{pcq} VM/2 = 0.5\%$) (7, 47): (a) influence of various load paths; (b) friction stress (Σf) and back stress (X) components ($R = \Sigma f + k_0$, k_0 initial yield stress).

to a γ' diameter of about 10 nm, and the overaged state (OA) to a γ' diameter $\phi = 150$ nm (6). Under proportional cyclic tests a strong Bauschinger effect is expected to occur for the overaged state (6). Figure 7(b) clearly shows the influence of the precipitate size on the back stress (X). It was reported elsewhere (45) that the Orowan by-passing process around large particles enhances the back stress component. It is now interesting to examine the mechanical behaviour in such alloys under complex loading paths. Whatever the loading path, it is observed that an increase of the phase lag goes hand-in-hand with an increase in the equivalent cyclic stress, Fig. 5(a), (46, 47). It was reported that this overstrengthening effect is associated with slip multiplicity (4, 6, 7, 48). Nevertheless comparing the slip multiplicity of the two conditions of the alloy, Fig. 5(b), would suggest a similar behaviour whatever the precipitate size. Figure 7(b) clearly shows that the overstrengthening effect proceeds mainly from either a friction stress component increase (UA state) or from both the X component and the friction stress component (OA state).



[b]	ATC	TTQ
U.A. $k = 850 \text{ MPa}$	$\Sigma_{eq} VM = 473 \text{ MPa}$ $R = -14 \text{ MPa}$ $X = 117 \text{ MPa}$	$\Sigma_{eq} VM = 522 \text{ MPa}$ $R = 54 \text{ MPa}$ $X = 98 \text{ MPa}$
O.A. $k = 580 \text{ MPa}$	$\Sigma_{eq} VM = 423 \text{ MPa}$ $R = 33 \text{ MPa}$ $X = 138 \text{ MPa}$	$\Sigma_{eq} VM = 501 \text{ MPa}$ $R = 128 \text{ MPa}$ $X = 121 \text{ MPa}$

Fig 8 Cyclic behaviour of 2024 aluminium alloy ($\Delta \epsilon_{peq} VM/2 = 0.35\%$) (6): (a) influence of various loading paths; (b) friction stress (Σf) and back stress (X) components ($R = \Sigma f + k_0$, k_0 initial yield stress).

The slip multiplicity concept no longer applies in such experiments. In our opinion, the back stress component increase under a 90° phase lag in the OA state proceeds from two phenomena i.e. the latent hardening and the γ' shape evolution during straining (Fig. 6). The γ' shape is less modified under complex loading paths, Fig. 6(b), which would enhance the back stress. As a matter of fact such an evolution in shape strongly suggests a more appropriate writing of the back stress on the slip systems instead of the phenomenological law generally used.

All results obtained for Waspaloy are gathered in Fig. 6; two remarks must be noted.

- (i) Overstrengthening effect for the underaged state is a transient phenomenon followed by a drastic softening, Fig. 7(a);

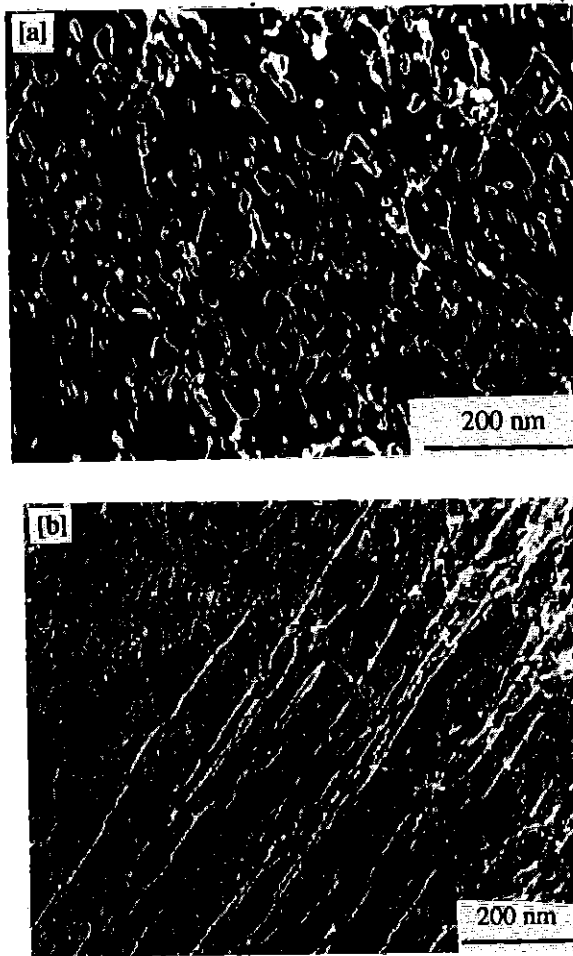


Fig 9 Deformation modes in 2024 aluminium alloy (6): (a) in-phase tests, dislocation loops; (b) out-of-phase tests, Lomer locks.

- (ii) Some particular loading paths (butterfly) lead to an overstrengthening effect greater than that obtained with a 90° out-of-phase. To our knowledge at the present time only a micro-macro approach (9) can account for such a complex effect above all in the case of the butterfly test. The physical basis of the overstrengthening is not clearly understood in terms of stress partitioning. Nevertheless, it was found that the butterfly test enhances slip multiplicity (47).

The mechanical behaviour of the aluminium alloy 2024 was also studied (underaged and overaged states). Unlike pure aluminium (10) it was shown that

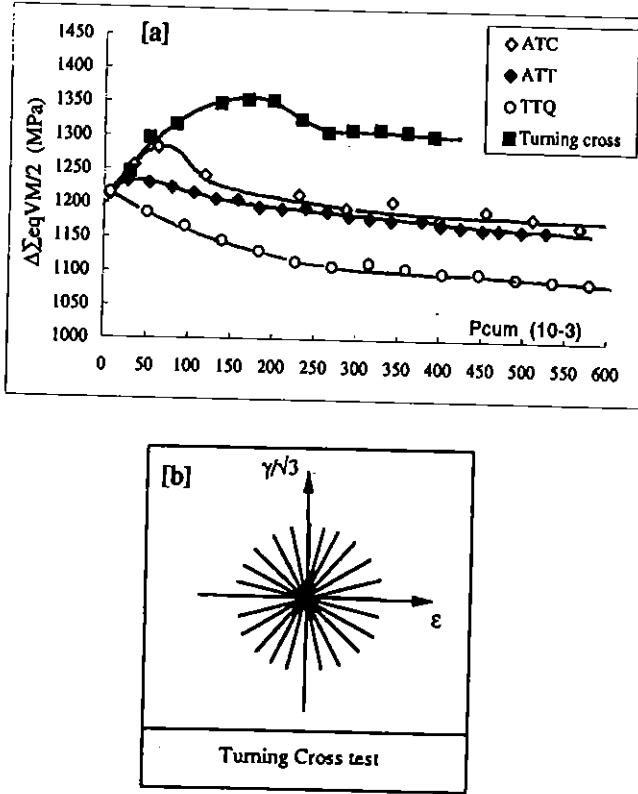


Fig 10 Mechanical behaviour of titanium alloy Ti-6246 (50): (a) influence of the loading path; (b) influence of the loading path; (b) definition of turning cross-test in $(\epsilon, \gamma/\sqrt{3})$ space.

a slight overstrengthening effect appears whatever the heat treatment in 2024, Fig. 8(a) (7, 47). The associated deformation modes i.e. dislocation loops spread in the matrix and Lomer lock formation, are related to slip multiplicity which is enhanced by non-proportional loading paths (Fig. 9). 2024 alloy dislocation features are the results of dislocation/precipitate interactions and of the influence of copper and magnesium atoms on planar slip via the stacking fault energy. Meanwhile in that case the overstrengthening effect results mainly from the friction stress component behaviour whatever the heat treatment used.

By comparing the mechanical behaviour of the two overaged alloys (Waspaloy and 2024) the influence of a very localized slip is demonstrated. In 2024 alloy the mean free path of dislocations is of the same order of magnitude as the average distance between precipitates and in that case S' precipitates do not actually experience dislocation by-passing. Localized slip will favour a very large mean free path so numerous dislocation loops are expected to appear around S' precipitates. The influence of the back stress on the overstrengthening effect in both alloys agrees fairly with the preceding microstructural remarks.

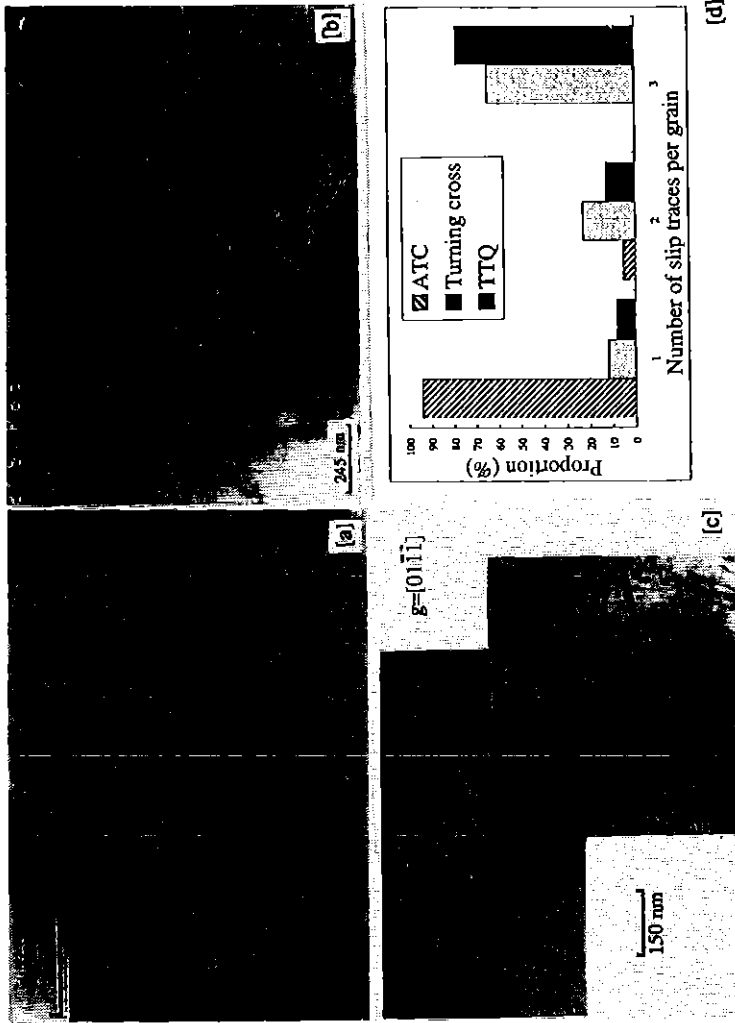


Fig 11 Deformation modes in 6246 Ti alloy (50); (a) in-phase test; (b) out-of-phase test; (c) turning cross-test; (d) the number of activated prism systems in α platelets.

BCC Structures

Very few results are available on BCC alloys which were tested at ambient temperature and under low applied strains; the mechanical behaviour would depend on sessile screw dislocations and Cottrell atmospheres. Under high applied strains or at high temperatures, the mechanical behaviour is expected to be similar to that observed for FCC alloys (49).

Dual-phase Alloys

Some results were reported on the behaviour of complex alloys such as dual-phase alloys or α/β titanium alloys under complex cyclic loadings. In our opinion these results show that physical parameters used in the first part no longer apply to such materials. The tests reported here were carried out on a titanium alloy α/β (α -phase HCP and β -phase BCC). In this alloy, localized slip is enhanced in the α -phase by Ti_3Al precipitates (50). The experimental procedure involves a 90° out-of-phase test and a turning cross-test (see reference (51) and Fig. 10). Softening occurs in this alloy under proportional loading path; the 90° out-of-phase test enhances this effect, whereas this effect vanishes under the turning cross-test. It appears that to turn around the elastic domain or to cross through it would induce a very different mechanical response. It is worth emphasizing that a similar remark could be made on the butterfly test on Waspaloy (9). From cyclic stress partitioning it appears that the back stress component bears the main part of the mechanical response (Table 5) (51).

Table 5 Mechanical parameters and stress partitioning results in 6246 titanium alloy (50)

	$P_{cum} (10^{-3})$	$\Delta\epsilon_{peq} VM/2$	$\Delta\Sigma_{eq} VM/2$ (MPa)	$\Delta X_{eq} VM/2$ (MPa)	$\Delta\Sigma_{res} VM/2$ (MPa)
ATC	400	7×10^{-3}	1177	618	559
TTQ	400	7×10^{-3}	1096	—	—
Turn. cross	400	7×10^{-3}	1311	756	555
ATC	2000	3×10^{-3}	1097	544	553
TTQ	2000	$3E - 3$	1003	453	550

From deformation modes studies it was observed that deformation proceeds only by prismatic slip system activation whatever the loading path. As expected, complex loadings enhance slip multiplicity (Fig. 11) whereas the slip multiplicity remains similar under the 90° out-of-phase test and the turning cross-test. The decrease in the X component under proportional loading was previously explained (50). It proceeds by progressive exhaustion of the back stress at the α/β interface whose source is a strong localized slip and/or a progressive multiplication of a strong localized slip band in the interior of a platelet. A two-phase approach, similar to the one used previously by others (23), allows a fairly good modelling of the mechanical behaviour of this alloy at the microscopic level. Nevertheless the understanding of differences which arise

between the 90° out-of-phase test and the turning cross-test remains to be acquired. We are at the present time working on this, and the results will be presented later.

Conclusion

In the present paper it is shown that the ratio $\gamma/(\mu b)$ can account for the mechanical behaviour of FCC metals. Overstrengthening ability increases as cross-slip propensity decreases. Nevertheless this approach no longer applies to some complex industrial metals and a partitioning of cyclic stress into back stress and friction stress must be done to obtain a better understanding of the overstrengthening phenomenon. Complex materials like α/β titanium alloys exhibit a specific sensitivity to non-proportional loading paths related to back stress evolution. In a wide range of materials (like BCC and HCP alloys) very large domains on the influence of complex loading paths on mechanical behaviour remain unexplored.

References

- (1) NITTA, A., OGATA, T., KUWABARA, K. (1989), Fracture mechanisms and life assessment under high strain biaxial cyclic loading of 304 stainless steel, *Fat. Fract. Engng. Mater. Struct.*, **12**, (2), pp. 77-92.
- (2) DOQUET, V. (1989), Comportement et endommagement de deux aciers à structure cubique centrées en fatigue obligocyclique sous chargement multiaxial non-proportionnel, doctoral thesis, ENSMP, France.
- (3) ITOH, T., SAKANE, M., OHNAMI, M., AMEYAMA, K. (1992), Additional hardening due to non-proportional cyclic loading. A contribution of stacking-fault-energy, *Pro. of Mecamat 92, Int. Sem. on Multiaxial Plasticity*, Cachan, France, pp. 43-50.
- (4) CLAVEL, M., PILVIN, P., RAHOUDJ, R. (1989), Analyse microstructurale de la déformation plastique sous sollicitations non-proportionnelles dans un alliage base nickel, *C.R. Acad. Sci. Paris*, **309**, (11), p. 689.
- (5) BEYLAT, L. (1991), Etude des modes de déformation d'alliages d'aluminium sous sollicitation monotone et cyclique (chargement proportionnel et non-proportionnel), doctoral thesis, UTC, France.
- (6) FERNEY, V., HAUTEFEUILLE, L., CLAVEL, M. (1991), Influence de la microstructure sur l'écroutissage cyclique d'alliages à durcissement structural en sollicitations multiaxiales: Comportement de l'alliage AU4G1, Part. I, *Mem. et Etu. Scien. Rev. de Metall.*, June-August, p. 441.
- (7) FERNEY, V., HAUTEFEUILLE, L., CLAVEL, M. (1991), Influence de la microstructure sur l'écroutissage cyclique d'alliages à durcissement structural en sollicitations multiaxiales: Comportement de l'alliage Waspaloy, Part. II, *Mem. et Etu. Scien. Rev. de Metall.*, October, p. 679.
- (8) BENALLAL, A., MARQUIS, D. (1987), Constitutive equation for non-proportional cyclic elasto-viscoplasticity, *Trans. of the ASME*, **109**, p.326.
- (9) PILVIN, P. (1990), Approches multiéchelles pour la prévision du comportement anélastique des métaux, doctoral thesis, Paris VI, France.
- (10) DOONG, S. H., SOCIE, D. F., ROBERTSON, I. M. (1990), Dislocation substructures and non-proportional hardening, *Trans. of the ASME*, **112**, p. 456.
- (11) DE LOS RIOS, E. R., ANDREWS, R. M., BROWN, M. W., MILLER, K. J. (1989), Out-of-phase cyclic deformation fracture studies on 316 stainless steel, *Biaxial and Multiaxial Fatigue*, EGF 3, Mechanical Engineering Publications, London, pp. 659-682.
- (12) DE LOS RIOS, E. R., KANDIL, F. A., MILLER, K. J., BROWN, M. W. (1985), A metallographic study of multiaxial creep-fatigue behaviour in 316 stainless steel, *Multiaxial Fatigue*, ASTM STP 853, American Society for Testing Materials, Philadelphia, pp. 669-687.

- (13) NISHINO, S., HAMADA, N., SAKANE, M., OHNAMI, M., MATSUMURA, N., TOKIZANE, M. (1986), Microstructural study of cyclic strain hardening behaviour in biaxial stress states at elevated temperature, *Fatigue. Fract. Engng. Mater. Struct.*, **9**, pp. 65–77.
- (14) DOONG, S. H. SOCIE, D. F. (1991), Deformation mechanisms of metals under complex non-proportional cyclic loading, *Fatigue under biaxial and multiaxial loading*, ESIS10, Mechanical Engineering Publications, London, pp. 305–320.
- (15) DOQUET, V., PINEAU, A. (1990), Extra hardening due to cyclic non-proportional loading of austenitic stainless steel, *Scripta Met. Mat.*, **24**, pp. 433–438.
- (16) MAGNIN, T., DRIVER, J., LEPINOUX, J., KUBIN, L. P. (1984), Aspects microstructuraux de la déformation cyclique dans les métaux et alliages C.C. et C.F.C.: I—Consolidation cyclique and II Saturation cyclique et localisation de la déformation, *Revue Phys. Appl.*, **19**, p. 467–502.
- (17) LEPINOUX, J. (1983), La déformation en sollicitation cyclique de monocristaux de cuivre, étude par microscopie électronique in situ, doctoral thesis, Univ. de Poitiers France.
- (18) MUGHRABI, H., WANG, R. (1981), Cyclic deformation of face-centred cubic polycrystals: a comparison with observations on single crystal, *Proc. of the 2nd Risø Inter. Symp. on Metall. and Mat. Sci.*, Eds. Hansen, N., Horsewell, A., Leffers, T., and Lilholt, H., pp. 87–98.
- (19) NEUMANN, P. (1983), Fatigue, *Physical Metallurgy*, Ed. Cahn, R. W. and Haasen, P., pp. 1553–1594.
- (20) L'ESPERANCE, G., VOGT, J. B., DICKSON, J. I. (1986), The identification of labyrinth wall orientations in cyclically deformed ASI-SAE 316 stainless steel, *Mat. Sci. and Eng.*, **79**, pp. 141–147.
- (21) DICKSON, J. I., BOUTIN, J., L'ESPERANCE, G. (1986), An explanation of labyrinth walls in fatigued F.C.C. metals, *Acta Met.*, **34**, pp. 1505–1514.
- (22) GERLAND, M., MENDEZ, J., VIOLAN, P., AIT SAADI, B. (1989), Evolution of dislocation structures and cyclic behaviour of 316L-type austenitic stainless steel cycled *in vacuo* at room temperature, *Mat. Sci. and Eng.*, **A118**, pp. 83–95.
- (23) MUGHRABI, H. (1983), Dislocation wall and cell structures and long-range internal stress in deformed metal crystal, *Acta Met.*, **31**, pp. 1367–1379.
- (24) CHICOIS, J., FOUGERES, R., GUICHON, G., HAMEL, A., VINCENT, A. (1986), Mobilité des dislocations lors de la sollicitation cyclique de l'aluminium polycristallin, *Acta Met.*, **34**, pp. 2157–2170.
- (25) GENTZBITTEL, ESNOUF, C., FOUGERES, R. (1987), Interactions between dislocations and crystalline during the cyclic deformation of 0.7% wt% Al—Li alloy, *Journal de Physique*, Col. C3, supp. no. 9, **48**, pp. 721–727.
- (26) MECKE, K., BLOCHWITZ, C. (1982), Saturation dislocation structures in cyclically deformed nickel single crystals of different orientations, *Crystal Res. and Technol.*, **17**, pp. 743–758.
- (27) FELTNER, C. E., LAIRD, C. (1968), Factors influencing the dislocation structures in fatigued metals, *Trans. of the AIME*, pp. 1253–1257.
- (28) COULOMB, P., *Scripta Met.* (1981), Comment on graphs relating some property to stacking fault energy, **15**, pp. 769–770.
- (29) BRECHET, Y. (1987), Fatigue des alliages binaires aluminium-lithium: un exemple de localisation de la déformation plastique, doctoral thesis, INP grenoble, France.
- (30) CAILLETAUD, G., DOQUET, V., PINEAU, A. (1991), Cyclic multiaxial behaviour of an austenitic stainless steel: microstructural observations and micromechanical modelling, *Fatigue under Biaxial and Multiaxial Loading*, ESIS10, Mechanical Engineering Publications, London, pp. 131–149.
- (31) TANAKA, E., MURAKAMI, S., OOKA, M. (1985), Effects of plastic amplitudes on non-proportional cyclic plasticity, *Acta Mech.*, **57**, pp. 167–182.
- (32) DOQUET, V., CLAVEL, M. (1996), Stacking-fault energy and cyclic hardening of F.C.C. solid solutions under multiaxial non-proportional loadings, *Multiaxial Fatigue and Design*, Mechanical Engineering Publications, London, pp. 43–60.
- (33) FRANCIOSI, P. (1985), The concepts of latent hardening and strain hardening in metallic single crystals, *Acta Met.*, **33**, pp. 1601–1612.
- (34) MURAKAMI, S., KAWAI, M., AOKI, K., OHMI, Y. (1989), Temperature dependence of multiaxial non-proportional cyclic behaviour of type 316 stainless steel, *Trans. of ASME*, **111**, pp. 32–39.
- (35) CLEMENT, N. (1984), Influence de l'ordre à courte distance sur les mécanismes de déformation des solutions solides, in *Ordre et désordre dans les matériaux*, Ed. de Physique, Ecole

- d'été-Aussois, France, pp. 167–182.
- (36) GEROLD, V., KARNTHALER, H.P. (1989), On the origin of planar slip in F.C.C. alloys, *Acta Met.*, **37**, pp. 2177–2183.
- (37) HONG, S. I., LAIRD, C. (1990), Mechanisms of slip mode modification in F.C.C. solid solutions, *Acta Met.*, **38**, pp. 1581–1594.
- (38) CAILLETAUD, G. (1987), Une approche micromécanique phénoménologique du comportement inélastique des métaux, doctoral thesis, Paris VI.
- (39) POLAK, J., KLESNIL, M., HELISIC, J. (1979), Stress dip technique for effective stress determination in cyclic straining, *Scripta Met.*, **13**, pp. 847–850.
- (40) ABEL, A., CHUNG, Y. S. (1979), Effective stresses in cyclic deformation, *Scripta Met.*, **13**, pp. 907–910.
- (41) COTTRELL, A. H. (1953), *Dislocations and Plastic Flow in Crystals*, Oxford University Press, London, pp. 111–116.
- (42) KULHMANN-WILSDORF, D., LAIRD, C. (1979), Dislocation behaviour in fatigue: II Friction stress and back stress as inferred from an analysis of hysteresis loops, *Mat. Sc. Eng.*, **37**, pp. 111–120.
- (43) DICKSON, J. L., BOUTIN, J., HANDEFIELD, L. (1984), A comparison of two simple methods for measuring cyclic internal and effective stresses, *Mat. Sc. Eng.*, **64**, L7–L11.
- (44) DOQUET, V. (1993), Twinning and multiaxial cyclic plasticity of a low stacking-fault-energy F.C.C. alloy, *Acta Metall. Mater.*, **41**, pp. 2451–2459.
- (45) BROWN, L. M., STOBBS, W. M. (1971), The work-hardening of copper-silica: II The role of plastic relaxation, *Phil. Mag.*, **23**, pp. 1201–1233.
- (46) VOISIN, J. M. (1989), Etude des relations entre microstructure et comportement mécanique du Waspaloy à température ambiante, DEA report ENSMP, France.
- (47) HAUTEFEUILLE, L., FERNEY, V., CLAVEL, M., PILVIN, P., CAILLETAUD G. (1992), Mechanical and microstructural modelling under multiaxial loading: application to 2024 alloy and to Waspaloy, *Proc. of Mecamat 92, Int. Sem. on Multiaxial Plasticity*, Cachan, France.
- (48) FERNEY, V. (1994), Etude de l'écroutissage cyclique sous sollicitations complexes (cas d'alliages à durcissement structural), doctoral thesis, UTC, France.
- (49) DOQUET, V., LE, T. N. (1993), private communication.
- (50) BERANGER, A. S., FEAUGAS, X., CLAVEL, M. (1993), Low cycle fatigue behaviour of an $\alpha + \beta$ titanium alloy: Ti-6246, *Mat. Sci. and Eng.*, **A1172**, pp. 31–41.
- (51) FEAUGAS, X. (1994), Microstructure et modélisation du comportement en fatigue uniaxiale et multiaxiale d'un alliage de titane biphasé, doctoral thesis, UTC, France.